geosciences

MDPI

Article

Sonar Estimation of Methane Bubble Flux from Thawing Subsea Permafrost: A Case Study from the Laptev Sea Shelf

Denis Chernykh [1,*], Vladimir Yusupov [2], Aleksandr Salomatin [1,*], Denis Kosmach [1], Natalia Shakhova [3,4], Elena Gershelis [5], Anton Konstantinov [1], Andrey Grinko [5], Evgeny Chuvilin [6], Oleg Dudarev [1], Andrey Koshurnikov [4] and Igor Semiletov [1,5,7]

1 V.I. Il'ichev Pacific Oceanological Institute, Far Eastern Branch of the Russian Academy of Sciences, 690041 Vladivostok, Russia; den-kosmach@mail.ru (D.K.); toshic.konstantinov@gmail.com (A.K.); dudarev@poi.dvo.ru (O.D.); ipsemiletov@alaska.edu (I.S.)
2 Research Center "Crystallography and Photonics" RAS, Institute of Photonic Technologies, 108840 Moscow, Russia; iouss@yandex.ru
3 International Arctic Research Center, University of Alaska Fairbanks, Fairbanks, AK 99775-7320, USA; nataliafletcher@yahoo.com
4 Scientific Centre Moscow State University (MSU)-Geophysics, 119234 Moscow, Russia; koshurnikov@msu-geophysics.ru
5 Department of Geology, Tomsk Polytechnic University, 634050 Tomsk, Russia; elenapanova@tpu.ru (E.G.); grinko@tpu.ru (A.G.)
6 Skolkovo Institute of Science and Technology, 121205 Moscow, Russia; E.Chuvilin@skoltech.ru
7 Institute of Ecology, National Research University Higher School of Economics, 111033 Moscow, Russia
* Correspondence: denis.chernykh.vl@gmail.com (D.C.); salomatin@poi.dvo.ru (A.S.)

Received: 26 September 2020; Accepted: 12 October 2020; Published: 14 October 2020

Abstract: Seeps found offshore in the East Siberian Arctic Shelf may mark zones of degrading subsea permafrost and related destabilization of gas hydrates. Sonar surveys provide an effective tool for mapping seabed methane fluxes and monitoring subsea Arctic permafrost seepage. The paper presents an overview of existing approaches to sonar estimation of methane bubble flux from the sea floor to the water column and a new method for quantifying CH_4 ebullition. In the suggested method, the flux of methane bubbles is estimated from its response to insonification using the backscattering cross section. The method has demonstrated its efficiency in the case study of single- and multi-beam acoustic surveys of a large seep field on the Laptev Sea shelf.

Keywords: active acoustic survey; seeps; permafrost; taliks; Laptev sea; East Siberian Arctic Shelf

1. Introduction

Release of previously generated methane (CH_4) preserved in natural gas fields, coal beds, and seabed deposits of CH_4 hydrates provides an important feedback in the Arctic climate system. Until recently [1], the Arctic Ocean was not considered as a possible source of CH_4 flux, as the impermeable subsea permafrost was believed [2] to seal marine sediments and prevent methane leakage to the water column and on to the atmosphere from the Arctic seabed which may store significant CH_4 reserves [3,4], including those sequestered in gas hydrates [5]. The permafrost of the East Siberian Arctic Shelf (ESAS), which makes up at least 80% of total subsea permafrost, has trapped the largest hydrocarbon reservoir on the planet [3,6,7]. However, the stability of the sequestered carbon (primarily in CH_4) is highly uncertain. Onshore and offshore Arctic permafrost can thaw from the top downward and bottom up. The downward degradation, with the respective expansion of the active layer, produces

unfrozen zones (taliks) which can also degrade from below under the effect of geothermal heat flux from underlying unfrozen sediments [8,9]. Thawing from below most often occurs in offshore seabed permafrost [2]. The ongoing warming in the Arctic is especially pronounced over ESAS, where the mean surface air temperature became up to 5 °C higher [10] for the first five years of the 21st century. The permafrost degradation may cause destabilization and dissociation of gas hydrates which can release large amounts of free gas.

The permafrost within ESAS features distinct zones serving as conduits for methane transmission [11] and causing in year-round round methane emission to the atmosphere from the sedimentary reservoir [1,12]. The daily bubble-mediated methane flux from large ESAS seeps can reach hundreds of grams per square meter [12,13]. This makes ESAS a significant modern marine source of CH_4, contributing to the regional methane budget as much as the terrestrial Arctic ecosystems [11]. The ESAS contribution to atmospheric CH_4 may be even greater, given its area (up to an order of magnitude larger than the Siberian wetlands) and methane emissions throughout winters, when terrestrial ecosystems are dormant [7,12]. Methane emissions in the ESAS are controlled by permafrost degradation, and the future emissions are expected to depend on the coastward dynamics of the subsea permafrost. The amount of CH_4 stored within the shallow ESAS seabed and the apparently widespread thawing of the subsea permafrost suggest that ESAS emissions may increase by 3–5 orders of magnitude [12,14]. The daily bubble-mediated methane flux from large ESAS seeps (Figure 1) can reach hundreds of grams per square meter [12,13]. Seeps in the Arctic shelf mark the areas of permafrost thawing and related destabilization of gas (methane) hydrates.

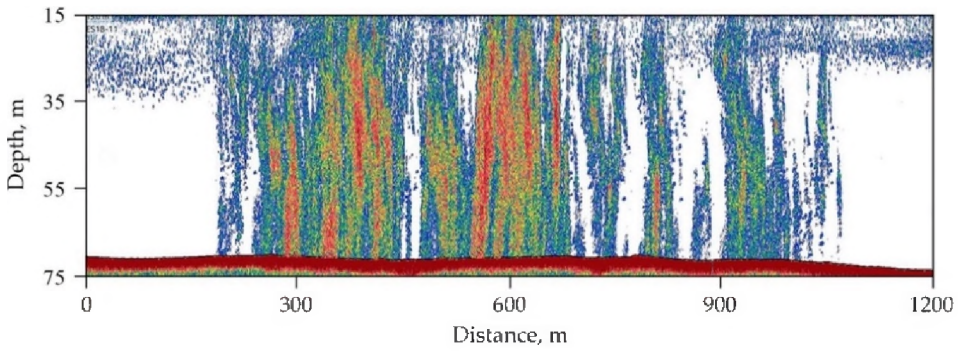

Figure 1. Sonar cross-section of seeps in the Arctic shelf.

Given the ESAS seepage extent there is a critical need for new effective, rapid, and quantitative monitoring approaches. Sonar surveys provide an effective tool for mapping seabed methane fluxes and monitoring subsea Arctic permafrost seepage driven by permafrost degradation. In this paper we report the results of single- and multi-beam acoustic surveys we undertook for quantifying CH_4 ebullition in the ESAS region [12,13].

2. Materials and Methods

Term gas seep is used in this study to refer to the release of gas in bubbles that rise from the seabed and form stable regions of increased bubble concentration in the water column. Seeps exist in shallow water on the shelf [1,15–18] or in deepwater offshore regions [15,19–21]. Each shallow seep occupies a few square km of the sea floor [12,22], while the deepwater seeps are commonly focused within 10 m (point seeps) and dispersed to large distances [15,16,20,21]. The single point seeps, mainly in deep sea, detectable separately by echo sounding are characterized by the flux F, which is the amount of methane carried by rising bubbles from a seep through a horizontal surface per unit time. The densely clustered shallow seeps, which are irresolvable individually, are characterized by the flux Fs from a unit area corresponding to the amount of methane carried by rising bubbles through a horizontal unit area per unit time.

2.1. Evaluation of Gas Flux within Water Column Using Sonar: Theoretical Background

Quantifying a methane bubble flux from sonar data is challenging and poorly amenable to laboratory modeling. Currently the problem has been solved by combined theoretical calculations, laboratory testing, and field experiments [12,13,15,22–28]. We consider several methods of remote active sonar estimation of bubble methane fluxes based on data from ship-mounted single- and multibeam echosounders operated in a monostatic mode when the acoustic transmitter also acts as a receiver. In this approach, the capacity of a physical object (including bubbles) to reflect and scatter the transmitted sound back to the receiver can be estimated via its backscattering cross section [29], with an area dimension:

$$\sigma_{bs} = \frac{I_{bs} L^2}{I}$$

where I_{bs} is the strength of the scattered signal at the receiver; L is the distance between the transmitter/receiver and the target; I is the strength of the original incident wave. The total (differential) backscattering cross section can be expressed logarithmically as the target strength TS of scatterers in the insonified volume [29,30]:

$$TS = 10 \cdot \frac{lg\sigma_{bs}}{A_1}$$

where $A_1 = 1$ m^2 is the unit area.

Single bubbles in ebullition zones monitored remotely by echo sounding (sonar) surveys are either resolvable (1) or not (2) in the acoustic data. The flux of methane into water and air due to resolvable single bubbles, which are often quite weak shallow sources [23], can be estimated from their rise velocity and size [15,16,31,32]:

$$F_s = \frac{1}{V_m \cdot t \cdot S} \sum_{i=1}^{N} \vartheta_i$$

where V_m is the molar volume of methane at the pressure and temperature of the respective sea depth; S is the insonified area at the given depth; N is the number of bubbles that cross the given surface for the time of observation t; ϑ_i is the volume of the i-th bubble [15] or

$$F_s = \frac{\langle V_b(r) \rangle \cdot P(h) \cdot N_b}{R \cdot T \cdot t \cdot S}$$

where $V_b(r)$ is the volume of a presumably spherical bubble with the radius r; $\langle\ \rangle$ is the averaging operator; $P(h)$ is the pressure at the sea depth h; N_b is the number of detected bubbles; t is the observation time; R is the gas constant; T is the Kelvin temperature °K [28]. The insonified area at the given distance L is given by

$$S = L^2 \cdot \Psi_D$$

where Ψ_D is the integrated beam width [29]:

$$S = \oint_{4\pi} D^2 d\Omega$$

D is the transducer range and $d\Omega$ is the solid angle increment.

The method is disadvantageous as it requires knowing the bubble size. The common single-beam echosounders cannot pinpoint single bubbles, which leads to large errors. Furthermore, the estimates of highly variable bubble sizes are poorly reliable because bubbles of different sizes can produce the same scattering patterns. Multi-frequency acoustic systems may help overcome this problem, but this solution is beyond the scope of our study.

More accurate backscattering cross-section estimates can be obtained with dual-beam (split-beam) echosounders [33] which use narrow and wide coaxial beams. In this case, calculations include only the scatterers recorded by both beams, and the target is located at the center of the wide beam used for

reference. The splitbeam sonars with complex antenna systems and additional phase measurements ensure the best performance [21,24,28,34].

The size of bubbles can be measured optically or inferred from their rise velocity, for instance, using graphical or empirical relationships [12,25,35], including in a special *Matlab* code [35]. The optical measurement is one of the best method to estimate bubble size, especially using sophisticated camera systems such as Wang et al. (2016) [36]. Nevertheless, these methods demand the chambers in close proximity to the bubbles being studied. Therefore, through it is very difficult, and often impossible, to examine in detail a large area with floating bubbles. However, these estimates of the size of bubbles by the second mentioned method are not very accurate for large bubbles (>1 mm radius) as their size poorly correlates with rise velocity. This velocity can be estimated only if single bubbles are resolvable by the sonar [15], when each bubble appears as an inclined line in the echogram, and the average velocity V is related to its slope as [15]:

$$V = \frac{\cos(\varphi)\cdot\Delta h}{\Delta t}$$

where Δh is the depth difference between the ends of the bubble path visible in the image; Δt is the respective time interval; φ is the beam half-width at the level equal to the ratio of signal amplitudes at the path ends to the maximum bubble response. At a high signal/noise ratio, this slope is close to zero beam width, which in common sonars approximately corresponds to 0.7. This equation is valid for the bubble sizes that do not change much for the observation time. The size dependence of the rise velocity [37] can be used to estimate the equivalent spherical radius r_i and hence the volume ϑ_i of each i-th bubble. The observed maximum height of gas plumes (also called flares) provides another tool for estimating bubble sizes [15,22,27]. It corresponds to the sea depth where the plumes are still seen in echograms as continuous zones of high scattering.

If single bubbles in a gas plume are irresolvable but their size, velocity, and shape distributions are known, the methane flux can be inferred from the total back scattering cross section [11,12,15,22,27,38,39], assuming that it equals the sum of cross sections for single bubbles, in the single scattering approximation [40]. In this approximation, the cross section of backscattering from a bubble cloud σ_{bs} is given by [29]:

$$\sigma_{bs} = N_0 \cdot \oint_0^\infty \sigma_{bsr}\cdot n(r)\cdot dr \quad (1)$$

where r is the bubble radius; N_0 is the number of bubbles in the cloud; $n(r)$ is the probability density function of the bubble size distribution; σ_{bsr} is the back scattering cross section of a single bubble of the radius r. The number N_0 depends on the number of bubbles (*i*) within the $h \pm l/4$ depth interval, where h is the sea depth and l is the pulse length in the case of deepwater gas plumes or single gas sources or (*ii*) within the segment of integrated beam width (Ψ_D) at a $h \pm l/4$ distance from shallow plumes or plumes rising from a dense cluster of irresolvable sources.

Closely spaced bubbles in large gas plumes, where the spacing between bubbles is commensurate with their radius, influence one another [38]. This interaction may reduce markedly the backscattering cross section and lead to underestimation of the respective gas flux values.

The bubble gas flux F (moles per second) is related with the size and shape distribution functions of $n(r)$ and $\Phi(r)$, respectively [15,27], as

$$F = \frac{N_0}{V_M}\cdot\frac{4\pi}{3}\cdot\int_0^\infty \Phi(r)\cdot V(r)\cdot r^3\cdot n(r)\cdot dr \quad (2)$$

where $V(r)$ is the rise velocity of bubbles.

Without N_0 in (1) and (2), the gas flux and the backscattering cross section become related as [28,33,41]:

$$F = \frac{1}{V_M} \cdot \frac{4\pi}{3} \cdot \frac{\int_0^\infty \Phi(r) \cdot V(r) \cdot r^3 \cdot n(r) \cdot dr}{\int_0^\infty \cdot \sigma_{bsr} \cdot n(r) \cdot dr} \cdot \sigma_{bs} = K \cdot \frac{\sigma_{bs}}{V_M} \quad (3)$$

where K is a complex distribution function of multiple variables: size, shape, rise velocity, surface, and acoustic properties of bubbles, as well as the sounding frequency, etc. Equation (3) defines the methane flux estimated from backscattering cross sections of deep-sea gas plumes or isolated point sources. In the case of multiple irresolvable sources, the flux from a unit area becomes

$$F_s = K \cdot \frac{\sigma_{bs}}{V_m \cdot S}$$

where S is the effective insonified area.

Thus, Equation (3) allows calculating the gas flux using the function K found from the known size, shape, and velocity distributions of bubbles, but these variables are often impossible to constrain. Therefore, the calculations are sometimes simplified by using the average values of the variables, assuming a spherical bubble shape.

For instance, the assumptions in [15] are that all bubbles have the same radius r and rise at the same velocity V; the radius of bubbles exceeds the resonance value; and $kr << 1$, where k is the wavenumber. With these assumptions, the methane flux (mole/s) is given by

$$F = \frac{8\pi \cdot r}{3 \cdot V_M \cdot l} \cdot V \cdot \sigma_{bs} \quad (4)$$

where V_M is the molar volume of methane at the temperature and pressure within the sounding depth, and l is the pulse length.

Otherwise, some variables are used as average values and others as approximating relationships, such as the exponential approximation of the bubble size distribution $n(r) = e^{-\alpha r}$ [28] that decreases stepwise to zero at $r \leq r_c$ (r_c is the smallest detectable size of bubbles; $r \geq r_c$ and $n(r) = 0$ at $r \leq r_c$). According to laboratory and field data, r_c is from 0.5 to 1.0 mm and $\alpha = 1.1$ mm^{-1}.

Note that the radii of the rising bubbles estimated as above are tentative. The size, shape, and velocity distributions of bubbles require more rigorous constraints, for example, by optical methods that allow direct measurements of these parameters for each bubble [12,22,25,35].

In all above solutions for the methane bubble flux, the backscattering cross section of a single bubble (σ_{bsr}) was found as

$$\sigma_{bsr} = \frac{r^2}{\left(\left(\frac{r_{res}}{r}\right)^2 - 1\right)^2 + \delta^2} \quad (5)$$

where r_{res} is the resonance radius of the bubble at the sonar operation frequency and δ is its damping factor. This is the most widespread approach in the sonar gas flux estimation practice [12,14,22,23,28]. Note that Equation (4) is valid at $kr \ll 1$, which imposes limitations on the sounding frequency. Strictly speaking, the 38 kHz frequency often used for methane flux estimation [21,28] is too high, because $kr = 1$ already at $r = 6$ mm. However, the validity of (5) can be extended into the $kr > 1$ domain to a satisfactory accuracy if the real nonspherical shape of bubbles is taken into account [27]. On the other hand, according to (5), the backscattering cross section of bubbles smaller than the resonance radius, decreases with decreasing bubble size at r^6, i.e., the contribution of these bubbles to the backscattered signal is vanishing, which is especially essential for deep-sea seeps. The resonance radius of bubbles is given by [27]:

$$r_{res} = \frac{1}{2\pi \cdot f_0} \cdot \sqrt{\frac{3 \cdot \gamma \cdot (P_0 + \rho_w g h}{\rho_w}} \quad (6)$$

where f_0 is the operation frequency; γ is the adiabatic exponent for gas in the bubble; P_0 is the atmospheric pressure; ρ_w is the water density; g is the acceleration due to gravity; h is the sea depth.

The resonance radii estimated with Equation (6) are 0.6 and 0.4 mm at a depth of 50 m (reached by the common 12 and 18 kHz sonar surveys), and 2.6 and 1.6 mm at 1 km. For shallow seeps, the frequency 18 kHz satisfies both conditions $kr \ll 1$ and $r_c \geq r_{res}$, as one can infer from the observed bubble sizes [12,25], though other frequencies, including hundreds of kHz, are applicable as well. The high-frequency systems are advantageous by being small, mobile, and energy-saving and thus convenient for research on various ships, even those that lack the mounted specialized equipment.

Choosing the sonar operation frequency for the responses of deep-sea seeps is more difficult as the range fitting both $r_c \geq r_{res}$ and $kr \ll 1$ decreases with depth, which may lead to large errors in the gas flux estimates.

Note that shallow seeps may pose additional problems due to strong resonance effects, as the attenuation $Q = 1/\delta$ of bubbles increases at decreasing pressure. The damping factor cannot exceed 7 at sea depths about 1000 m, where it is limited by the theoretical value associated with re-radiation, but it can reach a few tens at shallower <100 m depths [42]. Thus, the resonance effects increase markedly in the shallow sea, and the backscattering cross section of a single resonant bubble can be larger than that of several non-resonant ones.

Note that the simplifications used to estimate the bubble methane flux from backscattering cross section of a single bubble as in (5), with simplified approximations or average values instead of real size and rate distributions, are not always valid and may cause significant uncertainty. Furthermore, it is often impossible to choose the frequency fitting both $kr \ll 1$ and $r_c \geq r_{res}$ conditions, especially in the case of deep-sea seeps. As for the responses of shallow seeps, a large error may result from poor accuracy of the Q factor of bubbles and approximated attenuation of acoustic waves, as well as from neglected shape distribution of bubbles. Therefore, it is important to obtain rapid estimates of K in (3) in the conditions most similar to the real field surveys. Since this coefficient is a complex function of multiple variables, which are mostly unknown, the methods for obtaining its empirical rather than calculated values [12,13,22,34] are of special interest. So in work [34] on the basis of experiments with a horizontally looking single beam transducer (40 and 300 kHz) directed towards artificially produced bubbles, it was shown that an acoustic system can be calibrated in such a way that gas flux rates of bubble-size spectra, as observed at natural seeps, can be directly related to the echo level of a known, acoustically insonified volume.

2.2. Evaluation of Gas Flux within Water Column Using Sonar: Field Calibration Method

We estimated the methane bubble flux from the sea floor into the water column by a method similar to that in [34]. The main advantage of this approach is that the gas flux estimation does not require the knowledge of size, shape, and velocity distributions of bubbles and the specifications of the echosounder. Our method [12] differs from that suggested in [34] in two main aspects: the calibration in the field rather than in laboratory and vertical rather than horizontal insonification. The calibration was performed in typical local field conditions, while the vertical transmission and reception of signals was chosen since the methane flux was measured bottomward by ship-based echosounders. The measurements were run in the monostatic mode, as in [34], when the sonic waves are emitted and received by the same electroacoustic transducer. Since the transducer was submerged a few meters below the water surface, the distance L to the scattering volume was slightly less than its depth h. At the depth h, the echo is produced by rising bubbles within the effective scattering volume ΔV, which for $h \gg c\tau/2$ is given by [29]:

$$\Delta V \approx \frac{c\tau}{2} \cdot L^2 \cdot \Psi_D$$

where c is the sound speed; τ is the pulse duration; Ψ_D is the integrated beam width. The target strength within the effective scattering volume ΔV is described by the standard sonar equation [30]:

$$TS = RL - SL - TL \tag{7}$$

where TS is the target strength of bubbles within the effective scattering volume ΔV; RL is the received level, in dB/mPa; SL is the source level in the transmitter, in dB/mPa at 1 m; TL is the transmission loss due to spherical divergence and attenuation:

$$TL = 2 \cdot \left(20 \cdot log\left(\frac{L}{L_1}\right)\right) + \alpha L$$

where L_1 is the distance between the acoustic projector and the scattering bubbles (1 m) and α is the attenuation coefficient of the seawater, in dB/m. The received level is found as

$$RL = 10 \cdot log\left(U_n^2\right) + K_1$$

where U_n^2 is the normalized amplitude of the received signal for each ping n; K_1 is the constant depending on the parameters of the echosounder.

Commonly the modern sonars are designed to compensate the transmission losses. Thus, without TL and with constant SL, the TS equation becomes

$$TS = 10 \cdot log\left(U_0^2\right) + K_2$$

where K_2 is the calibration coefficient; U_0^2 is the normalized amplitude of each ping n at compensated transmission losses. Therefore, the methane flux from isolated seeps is

$$F = K_B \cdot \frac{U_0^2}{V_M} \tag{8}$$

The flux from unit area in shallow seeps, with acoustically irresolvable bubbles, is

$$F = K_B \cdot \frac{U_0^2}{V_M \cdot S} \tag{9}$$

where S is the effective scattering area.

As follows from (8), the calculations can be limited to simple calibration measurements of gas flux dependence of the backscatter strength for deep-sea seeps, but additional knowledge of angle parameters may be required to estimate the effective scattering area S by (9) in the case of irresolvable shallow seeps. This area is found from the distance between the projector and the insonified volume and from the integrated beam width Ψ_D. Unfortunately, the manufacturer does not provide Ψ_D values in the specifications. For a piston transducer, it can be estimated as [29]

$$\Psi_D = \frac{5.48}{(kr)^2}$$

where k is the wavenumber; r is the transmitter radius.

Analysis of multibeam records is worth special interest as they include backscattering strength in 3D, depth and period of emitted signals, as well as beam number of the multibeam system. The fragment of a multibeam sonar cross-section of a seep in Figure 2a shows distortions associated with propagation of a sonic wave that was transmitted and received at different angles to the vertical in the water column. In other words, a 90° incident signal will reach the 100 m depth before that emitted at 60°. The shift of the signal in depth (L) and insonified area (D) can be calculated from the known

sound speed (c), sampling rate (f_{qua}), beam number (n) and dip (α), and the distance (n) traveled by the signal, using Equations (10) and (11).

$$L = i \cdot \frac{c}{2 \cdot f_{qua}} \cos(n \cdot \alpha) \quad (10)$$

$$D = i \cdot \frac{c}{2 \cdot f_{qua}} \sin(n \cdot \alpha) \quad (11)$$

where c is the sound speed; f_{qua} is the sampling rate; n is the beam number; α is the beam dip; i is the distance traveled by the signal.

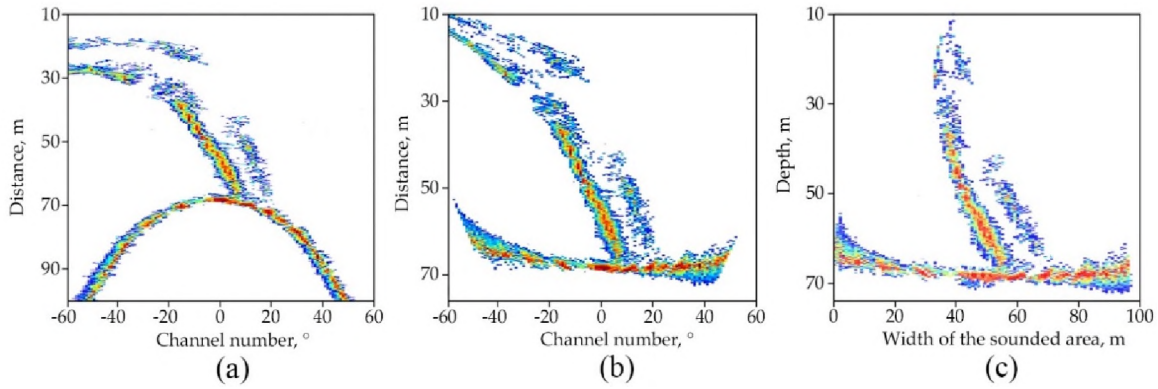

Figure 2. A multibeam sonar image before (**a**) and after (**b**,**c**) correction for the shift in depth (**b**) and insonified area (**c**).

The variables L and D, as well as the beam number n, should be added to Equations (4) and (9) for the bubble gas flux estimation.

2.3. Calibration of the Sonar

The survey campaign at a test site in the East Siberian Arctic shelf included calibration work in accordance with the project objectives: (i) standard procedure using a tungsten carbid target 38.1 mm in diameter and (ii) special calibration using an artificial sounder-derived gas plume. The data were processed in *MatLab*, with estimation of mean values and standard deviation. The match between different data populations was checked with the Student criterion ($p < 0.05$).

The standard calibration consisted in estimating the maximum square amplitude of the received signal U_0^2 that was backscattered by a target submerged to 4.5 m below the water surface in the middle of the insonified area, at user-specified sounding parameters (pulse frequency, amplitude, duration, etc.). The normalized amplitude U_0^2 represents each signal with compensated transmission losses, proceeding from the real distribution of temperature, salinity, and sound speed in the given place of the water column. The conductivity, temperature, and depth data were acquired with a *CastAway-CTD* probe within 100 m depths, at a sampling rate of 5 Hz, to an accuracy of ±0.1 PSU for salinity and ±0.05 °C for temperature. The strength TS of the calibration target was estimated as in [43–45] from temperature and salinity at the target depth (Figure 3a).

According to the frequency dependence of TS obtained by calibration of the Simrad EK15 echosounder (Figure 3b), the average TS is −39.18 dB/m^2, which corresponds to the σ_{bs0} = 1.21 cm^2 backscattering cross section of the calibration sphere.

The calibration provided constraints on the correlation K_0 between the target scattering cross section σ_{bs0} and the normalized square amplitude of the calibration signal:

$$K_0 = \frac{\sigma_{bs0}}{U_0^2}$$

Special calibration of the Simrad EK15 echosounder was performed using a gas plume produced by a bubble generator [12,13,22] consisting of several sequentially connected units: a gas bomb with nitrogen, a gas supply system with gas flux control, and a submerged nozzle with an outlet diameter of 3 mm; the flux rate was set in a range of 0.02 L/s to 1.27 L/s.

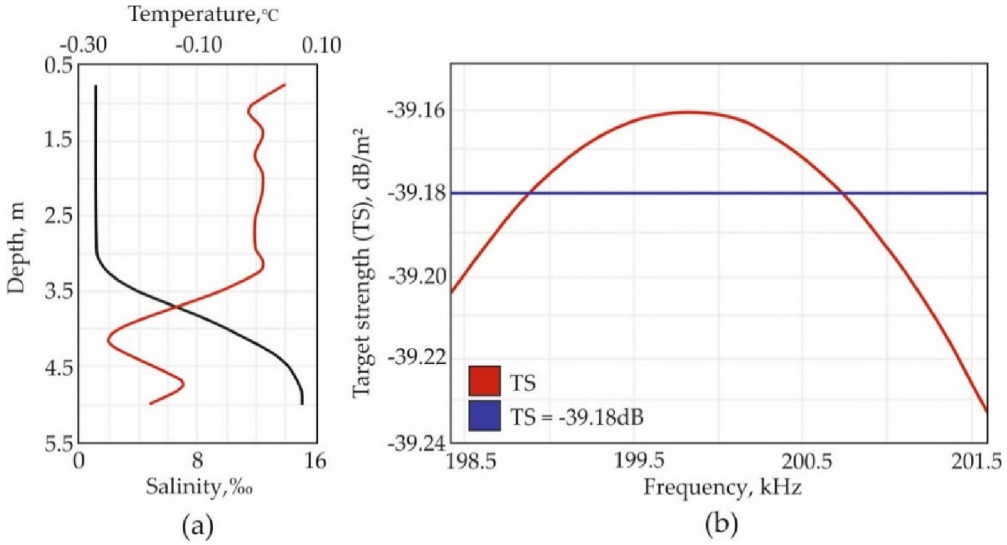

Figure 3. Simrad EK15 calibration: temperature and salinity profiles (**a**); observed (red line) and averaged (blue line) frequency dependence of target strength (*TS*) (**b**).

Calibration provided an empirical relationship between the backscattering strength at the depth ~39 m and the gas flux from a nozzle at the depth 40 m in the middle of the beam width. Since any gas other than methane can be used for calibration [13], we chose nitrogen, which is a safe inert gas. The diameter of bubbles estimated by direct optical measurements ranged from 3 to 12 mm and corresponded to the characteristic size of natural bubbles in seep sites [22,25,31].

2.4. Relationship between Gas Flux and Measured Response

The difference between the calibrations when using methane and nitrogen can be neglected, since for the densities of these gases of the used depths (39 m) are much lower than the density of water. For bubbles, the difference at different gas content is observed in the region of resonance frequencies. Since the operating frequencies are much higher than the resonant frequencies, this difference can be neglected. The difference in diffusion of these two gases can also be neglected, since measurements are taken near seabed. In addition, these depths are much higher than the zone of stability of methane gas hydrate (about 300 m), so the formation of a gas hydrate crust on the surface of the bubbles does not occur. The applied 200 kHz frequency was much higher than the resonance frequency of such bubbles and thus satisfied the calibration requirement. The calibration sonar cross-section of Figure 4a was obtained at a flow rate of 1.27 L/s and resolved well the sea floor and the zone of ebullition-related scattering in the water. The signal attenuated at depths shallower than ~15 m due to a strong near-surface current which dragged the rising bubbles outside the beam width.

The calibration curve (Figure 4b) represents the gas flux dependence of normalized square voltage at the echosounder output, with each point being a result of averaging over 420 pings in 7 min sampling intervals. The experimental points fit well the straight line through the origin of coordinates which records linear correlation between the signal (U_0^2) and the flux (F) in the used range from 1 to 57 mmol/s and thus confirms the validity of Equations (8) and (9) for a large range of gas fluxes. Therefore, the empirical coefficient K obtained in field conditions can make basis for rapid estimation of bubble methane fluxes without data on bubbles in gas plumes and echosounder specifications. This calibration method is applicable to multibeam sounders as well [9].

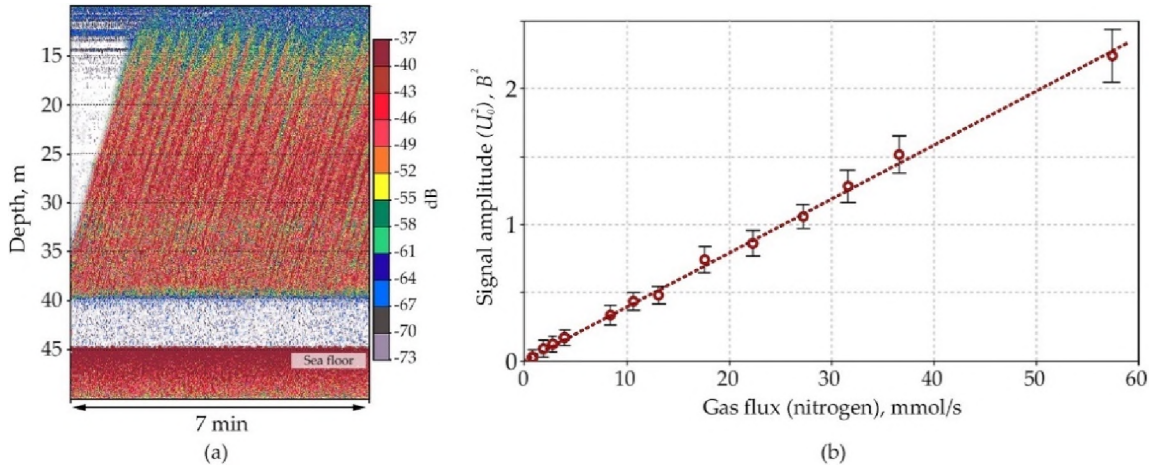

Figure 4. Sonar cross-section of an engineered seep detected during calibration (**a**); calibration curve of signal amplitude vs. bubble gas flux (**b**).

Note that in our case, the calibration was carried out for a source at a depth of 40 m. These data were extrapolated to other depths by introducing the values of the molar volume V_M and sonicated area into the Formula (9), recalculated for a given depth and temperature at the bottom.

3. Results and Discussion

Sonar estimation of bubble-mediated methane fluxes requires an operation frequency f exceeding the resonance frequency of rising bubbles f_r but low enough to reduce the damping of transmitted and echoed signals. We used a 200 kHz Simrad EK15 singlebeam echosounder with its frequency above the resonance values of bubbles at all selected sea depths from 0 to 100 m. This study covered area of the ESAS: the ice-free area of the Laptev Sea (between 76.5–77.5° N and 121–132° E, water depth between 50 and 165 m (Figure 5).

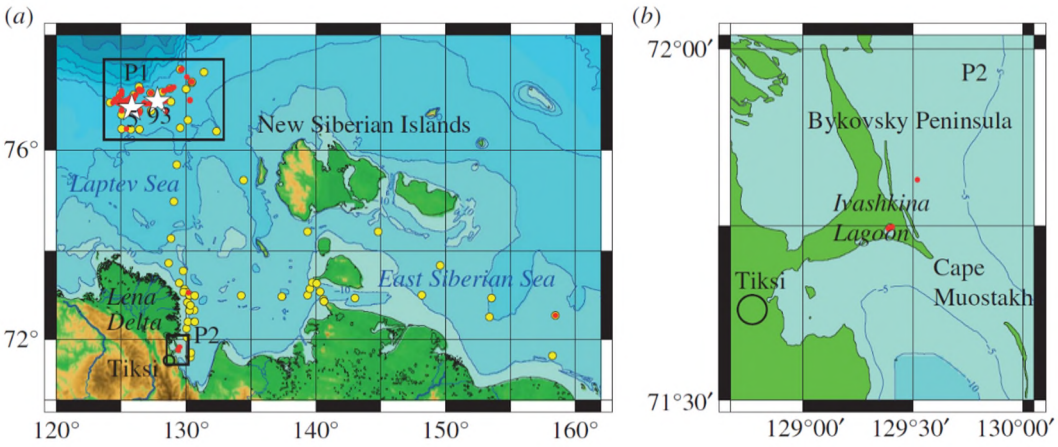

Figure 5. Study area. (**a**) Black rectangles mark the position of polygon 1 (P1, outer shelf) and polygon 2 (P2, near shore area); red circles show the position of discovered seep fields in the study area where hydro acoustical investigations were performed: white stars mark the position of two seep fields (F5 and F93) where detailed surveys were performed; yellow circles show the position of oceanographic stations in the study area; green shows land; blue shows water; bathymetry lines are shown as black counters; (**b**) the red circle shows position of the Ivashkina Lagoon within P2 [12].

The methane flux quantified from measured backscattering cross sections of bubbles in a large methane seep from the Laptev shelf [12] was compared with the results of calibration against an

engineered gas plume. The respective ebullition zone is clearly pronounced in the example sonar cross-section of Figure 6a.

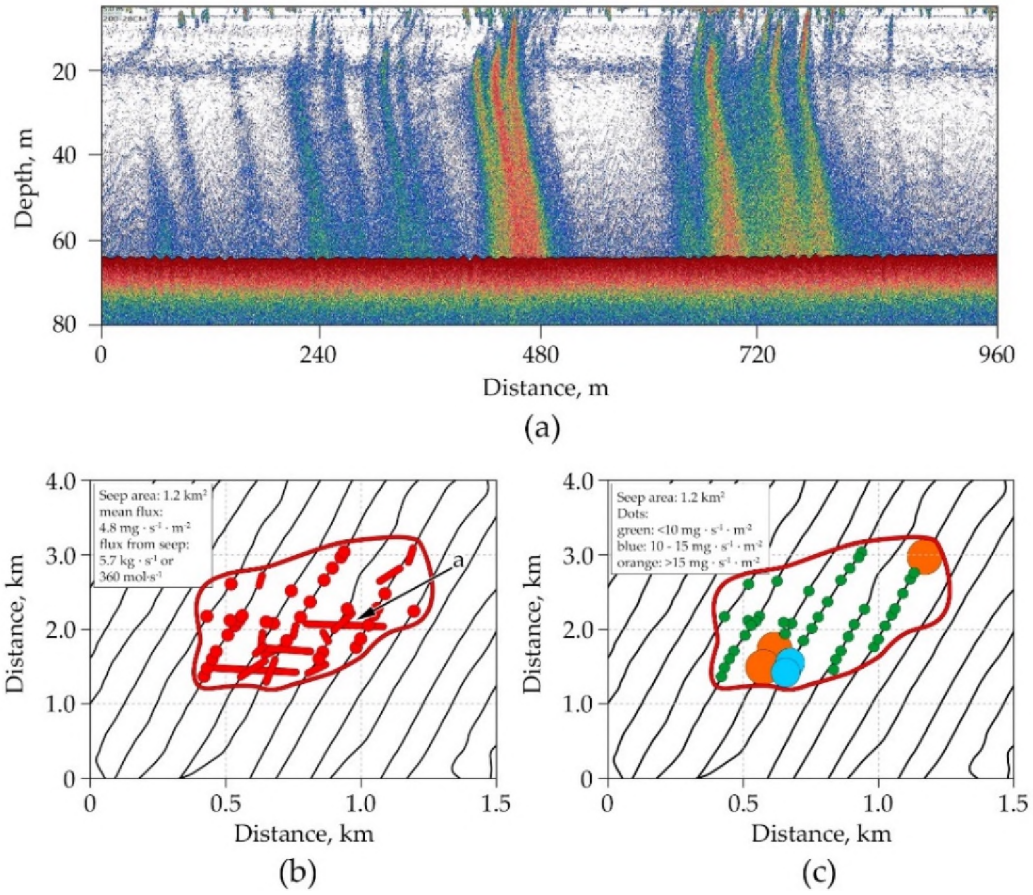

Figure 6. Singlebeam sonar image of a large seep in the Laptev Sea (**a**); location of methane seeps in the zone of ebullition (red dots) and Research Vessel tracks (black lines) tracks. Red lines show >100 m seeps (**b**); amount of methane released by each seep (**c**).

Echo sounding surveys of 49.7 km over a test area of 6 km^2 2018 in a region of a large methane seep discovered in 2011 [12,46] revealed 46 independent vents from 15 to 336 m in diameter, including 15 seeps larger than 100 m (Figure 6b). The seeps were found out to cover 1.2 km^2 and produce a gas flux of 5.7 ± 0.6 kg/s, as estimated from measured backscattering cross section and by calculations with Equation (4), using measured radius and rise velocity of bubbles; the >100 m seeps provide the greatest contribution to the total flux (Figure 6c). The estimates by Equation (9) using data calibrated against an artificial gas plume gave 6.8 ± 0.8 kg/s. The two gas flux values differ to 19%, at $p < 0.05$.

We also performed observations in the southernmost part of the Laptev Sea, in Ivashkina Lagoon, which has been progressively inundated during the last ~100–500 years, replacing a former thermokarst lake. Bubble release occurred from narrow, steep depressions aligned parallel to the lagoon's northern edge. Backscattering cross-sections of the bubbles emitted from 17 seeps observed in Ivashkina Lagoon were recorded for 36 h using portable single-beam sonar, which was calibrated in situ during the same campaign. In Ivashkina Lagoon, CH_4 fluxes observed in October 2013 ranged from 5 to 24 g m^{-2} d^{-1} [12].

Thus, the proposed method, based on the determination of the empirical coefficient K in field conditions, makes it possible to carry out a quick estimation of bubble methane fluxes without data on bubbles (distributions of size, shape and rise velocity) in gas plumes and echo sounder calibrations. This method is applicable to multibeam echo sounders as well.

4. Conclusions

Among several other reviewed approaches, the new method for sonar quantifying of methane ebullition in the water column based on calculations from the cross section of backscattering from rising CH_4 bubbles has been tested in a large seep area on the Laptev Sea shelf has demonstrated its efficiency. The gas flux estimates by the new method are comparable to those obtained by calibration against an engineered gas plume: 5.7 ± 0.6 and 6.8 ± 0.8 kg/s, respectively. Thus, both methods are applicable for rapid remote estimation of CH_4 fluxes from seeps, taking into account that the backscattering cross section may be about 20% lower than the true values.

Author Contributions: D.C., V.Y. and A.S.—methodology for sonar estimation of methane flux from the sea bed to the water; D.K., N.S., A.K.(Anton Konstantinov) and E.C.—conceptualization, methodology, and manuscript preparation; I.S., and O.D.—organization of echo sounding surveys and project coordination; E.G., A.K.(Andrey Koshurnikov) and A.G.—graphic visualization. All authors have read and agreed to the published version of the manuscript.

Funding: The research was supported by the Russian Science Foundation grants 18-77-10004 and 19-77-00067. Acknowledge the Russian Government (Grant No. 14, Z50.31.0012/03.19.2014). TPU Competitiveness Enhancement Program #VIU/OG-215/2020 and #VIU/OG-217/2020. The Grant of the President of the Russian Federation for state support of young Russian scientists—candidates of science (#MK-535.2020.5).

Acknowledgments: We wish to thank the crew of R/Vs *Victor Buynitsky*, *Akademik M.A. Lavrentiev*, and *Akademik Mstislav Keldysh* for support in echo sounding surveys.

Conflicts of Interest: The authors declare no conflict of interest.

References

1. Shakhova, N.; Semiletov, I.; Salyuk, A.; Yusupov, V.; Kosmach, D.; Gustafsson, O. Extensive Methane Venting to the Atmosphere from Sediments of the East Siberian Arctic Shelf. *Science* **2010**, *327*, 1246–1250. [CrossRef]
2. Romanovskii, N.; Hubberten, H.W.; Gavrilov, A.; Eliseeva, A.; Tipenko, G. Offshore permafrost and gas hydrate stability zone on the shelf of East Siberian Seas. *Geo Mar. Lett.* **2002**, *25*, 167–182. [CrossRef]
3. Soloviev, V.A.; Ginzburg, G.D.; Telepnev, E.V.; Mikhaluk, Y.N. *Cryothermia and Gas Hydrates in the Arctic Ocean*; Sevmorgeologia: Leningrad, Russia, 1987.
4. Kvenvolden, K.A. Methane hydrate—A major reservoir of carbon in the shallow geosphere? *Chem. Geol.* **1988**, *71*, 41–51. [CrossRef]
5. Kvenvolden, K. Gas hydrates—Geological perspective and global change. *Rev. Geophys.* **1993**, *31*, 173–187. [CrossRef]
6. Shakhova, N.; Semiletov, I.; Leifer, I.; Salyuk, A.; Rekant, P.; Kosmach, D. Geochemical and geophysical evidence of methane release over the East Siberian Arctic Shelf. *J. Geophys. Res. Ocean.* **2010**, *115*, C08007. [CrossRef]
7. Shakhova, N.; Semiletov, I.; Chuvilin, E. Understanding the Permafrost–Hydrate System and Associated Methane Releases in the East Siberian Arctic Shelf. *Geoscience* **2019**, *9*, 251. [CrossRef]
8. Osterkamp, T.E. Sub-Sea Permafrost. In *Encyclopedia of Ocean Sciences*, 2nd ed.; Steele, J.H., Ed.; Academic Press: Oxford, UK, 2001; pp. 559–569. [CrossRef]
9. Shakhova, N.; Semiletov, I.; Shakhova, N.E.; Semiletov, I.P. Methane Hydrate Feedbacks. In *Arctic Climate Feedbacks: Global Implications*; Sommerkorn, M., Hassol, S.J., Eds.; WWF International Arctic Programme: Gland, Switzerland, 2009; pp. 81–92. ISBN 978-2-88085-305-1.
10. State of the Arctic Report. Available online: http://editors.eol.org/eoearth/wiki/State_of_the_Arctic_Report (accessed on 12 August 2020).
11. Shakhova, N.; Semiletov, I.; Leifer, I.; Sergienko, V.; Salyuk, A.; Kosmach, D.; Chernykh, D.; Stubbs, C.; Nicolsky, D.; Tumskoy, V.; et al. Ebullition and storm-induced methane release from the East Siberian Arctic Shelf. *Nat. Geosci.* **2014**, *7*, 64–70. [CrossRef]
12. Shakhova, N.; Semiletov, I.; Sergienko, V.; Lobkovsky, L.; Yusupov, V.; Salyuk, A.; Salomatin, A.; Chernykh, D.; Kosmach, D.; Panteleev, G.; et al. The East Siberian Arctic Shelf: Towards further assessment of permafrost-related methane fluxes and role of sea ice. *Philos. Trans. R. Soc. A Math. Phys. Eng. Sci.* **2015**, *373*, 20140451. [CrossRef]

13. Leifer, I.; Chernykh, D.; Shakhova, N.; Semiletov, I. Sonar gas flux estimation by bubble insonification: Application to methane bubble flux from seep areas in the outer Laptev Sea. *Cryosphere* **2017**, *11*, 1333–1350. [CrossRef]
14. Shakhova, N.; Semiletov, I.; Gustafsson, O.; Sergienko, V.; Lobkovsky, L.; Dudarev, O.; Tumskoy, V.; Grigoriev, M.; Mazurov, A.; Salyuk, A.; et al. Current rates and mechanisms of subsea permafrost degradation in the East Siberian Arctic Shelf. *Nat. Commun.* **2017**, *8*, 15872. [CrossRef]
15. Salomatin, A.S.; Yusupov, V.I. Acoustic Investigations of Gas "Flares" in the Sea of Okhotsk. *Oceanology* **2011**, *51*, 857–865. [CrossRef]
16. Andreassen, K.; Hubbard, A.; Winsborrow, M.; Patton, H.; Vadakkepuliyambatta, S.; Plaza-Faverola, A.; Gudlaugsson, E.; Serov, P.; Deryabin, A.; Mattingsdal, R.; et al. Massive blow-out craters formed by hydrate-controlled methane expulsion from the Arctic seafloor. *Science* **2017**, *356*, 948–952. [CrossRef] [PubMed]
17. Vetrov, A.; Lobus, N.; Drozdova, A.; Belyaev, N.; Romankevich, E. Methane in Water and Bottom Sediments in Three Sections in the Kara and Laptev Seas. *Oceanology* **2018**, *58*, 198–204. [CrossRef]
18. Judd, A. The global importance and context of methane escape from the seabed. *Geo Mar. Lett.* **2003**, *23*, 147–154. [CrossRef]
19. Kasatkin, S.A.; Obzhirov, A.I. Fluid-Controlling Significance of the Nosappu Fracture Zone and Conditions for the Formation of Methane Fluxes and Gas Hydrates (Sea of Okhotsk Region). *Russ. J. Pac. Geol.* **2018**, *12*, 57–62. [CrossRef]
20. Shakirov, R.B.; Obzhirov, A.I.; Salomatin, A.S.; Makarov, M.M. New Data on Lineament Control of Modern Centers of Methane Degassing in East Asian Seas. *Dokl. Earth Sci.* **2017**, *477*, 1287–1290. [CrossRef]
21. Greinert, J.; Artemov, Y.; Egorov, V.; De Batist, M.; McGinnis, D. 1300-m-high rising bubbles from mud volcanoes at 2080 m in the Black Sea: Hydroacoustic characteristics and temporal variability. *Earth Planet. Sci. Lett.* **2006**, *244*, 1–15. [CrossRef]
22. Chernykh, D.V.; Yusupov, V.I.; Salomatin, A.S.; Kosmach, D.A.; Konstantinov, A.V.; Silionov, V.I.; Mazurov, A.K.; Salyuk, A.N.; Shakhova, N.E.; Gustafsson, O.; et al. New acoustical technique to quantify methane ebullition in sediment water column: A case study in the Laptev sea, the Arctic ocean. *Bull. Tomsk Polytech. Univ. Geo Assets Eng.* **2018**, *329*, 153–167.
23. Weidner, E.; Weber, T.C.; Mayer, L.; Jakobsson, M.; Chernykh, D.; Semiletov, I. A wideband acoustic method for direct assessment of bubble-mediated methane flux. *Cont. Shelf Res.* **2019**, *173*, 104–115. [CrossRef]
24. James, R.H.; Bousquet, P.; Bussmann, I.; Haeckel, M.; Kipfer, R.; Leifer, I.; Niemann, H.; Ostrovsky, I.; Piskozub, J.; Rehder, G.; et al. Effects of climate change on methane emissions from seafloor sediments in the Arctic Ocean: A review. *Limnol. Oceanogr.* **2016**, *61*, S283–S299. [CrossRef]
25. Makarov, M.; Muyakshin, S.; Kucher, K.; Aslamov, I.; Granin, N. A study of the gas seep Istok in the Selenga shoal using active acoustic, passive acoustic and optical methods. *J. Great Lakes Res.* **2020**, 46. [CrossRef]
26. Makarov, M.; Muyakshin, S.; Kucher, K.; Aslamov, I.; Gnatovsky, R.; Granin, N. Bubble gas escapes from the bottom of lake Baikal: Observation with help of the echosounder, estimation of methane flux and connection of this flux with bubble flare height. *Fundam. I Prikl. Gidrofiz.* **2015**, *9*, 32–41.
27. Salomatin, A.S.; Yusupov, V.I.; Vereshchagina, O.F.; Chernykh, D.V. An acoustic estimate of methane concentration in a water column in regions of methane bubble release. *Acoust. Phys.* **2014**, *60*, 671–677. [CrossRef]
28. Muyakshin, S.; Sauter, E. The hydroacoustic method for the quantification of the gas flux from a submersed bubble plume. *Oceanology* **2010**, *50*, 995–1001. [CrossRef]
29. Medwin, H.; Clay, C.S. *Fundamentals of Acoustical Oceanography*; Academic Press: San Diego, CA, USA, 1997; ISBN 978-0-12-487570-8. [CrossRef]
30. Urick, R.J. *Principles of Underwater Sound*, 3rd ed.; Peninsula Publishing: Westport, CT, USA, 1996.
31. Leifer, I.; Patro, R.K. The bubble mechanism for methane transport from the shallow sea bed to the surface: A review and sensitivity study. *Cont. Shelf Res.* **2002**, *22*, 2409–2428. [CrossRef]
32. Veloso, M.; Greinert, J.; Mienert, J.; De Batist, M. A new methodology for quantifying bubble flow rates in deep water using splitbeam echosounders: Examples from the Arctic offshore NW-Svalbard. *Limnol. Oceanogr. Methods* **2015**, *13*, 267–287. [CrossRef]
33. Munk, W.; Wunsch, C. Ocean acoustic tomography: A scheme for large scale monitoring. *Deep Sea Res. Part A Oceanogr. Res. Pap.* **1979**, *26*, 123–161. [CrossRef]

34. Greinert, J.; Nutzel, B. Hydroacoustic experiments to establish a method for the determination of methane bubble fluxes at cold seeps. *Geo Mar. Lett.* **2004**, *24*, 75–85. [CrossRef]
35. Leifer, I.; Culling, D. Formation of seep bubble plumes in the Coal Oil Point seep field. *Geo Mar. Lett.* **2010**, *30*, 339–353. [CrossRef]
36. Wang, B.; Socolofsky, S.A.; Breier, J.A.; Seewald, J.S. Observations of bubbles in natural seep flares at MC 118 and GC 600 using in situ quantitative imaging. *J. Geophys. Res. Ocean.* **2016**, *121*, 2203–2230. [CrossRef]
37. McGinnis, D.F.; Greinert, J.; Artemov, Y.; Beaubien, S.E.; Wuest, A. Fate of rising methane bubbles in stratified waters: How much methane reaches the atmosphere? *J. Geophys. Res.—Ocean.* **2006**, *111*, C09007. [CrossRef]
38. Maksimov, A.O.; Burov, B.A.; Salomatin, A.S.; Chernykh, D.V. Sounds of marine seeps: A study of bubble activity near a rigid boundary. *J. Acoust. Soc. Am.* **2014**, *136*, 1065–1076. [CrossRef] [PubMed]
39. Yusupov, V.I.; Salyuk, A.N.; Karnaukh, V.N.; Semiletov, I.P.; Shakhova, N.E. Detection of methane ebullition in shelf waters of the Laptev Sea in the Eastern Arctic Region. *Dokl. Earth Sci.* **2010**, *430*, 261–264. [CrossRef]
40. Ishimaru, A. *Wave Propagation and Scattering in Random Media*; Wiley: Hoboken, NJ, USA, 1999.
41. Granin, N.; Muyakshin, S.; Makarov, M.; Kucher, K.; Aslamov, I.; Granina, L.; Mizandrontsev, I. Estimation of methane fluxes from bottom sediments of Lake Baikal. *Geo Mar. Lett.* **2012**, *32*. [CrossRef]
42. Ainslie, M.; Leighton, T. Review of scattering and extinction cross-sections, damping factors, and resonance frequencies of a spherical gas bubble. *J. Acoust. Soc. Am.* **2011**, *130*, 3184–3208. [CrossRef]
43. Foote, K.G.; Knudsen, H.P.; Vestnes, G. Improved Calibration of Hydroacoustic Equipment with Copper Spheres. Available online: https://imr.brage.unit.no/imr-xmlui/bitstream/handle/11250/102773/CM_1981_B_20.pdf?sequence=1 (accessed on 17 August 2020).
44. MacLennan, D.N. *The Theory of Solid Spheres as Sonar Calibration Targets*; Department of Agriculture and Fisheries for Scotland: Edinburgh, Scotland, 1981.
45. MacLennan, D.N.; Dunn, J.R. Estimation of sound velocities from resonance measurements on tungsten carbide calibration spheres. *J. Sound Vib.* **1984**, *97*, 321–331. [CrossRef]
46. Sergienko, V.I.; Lobkovskii, L.I.; Semiletov, I.P.; Dudarev, O.V.; Dmitrievskii, N.N.; Shakhova, N.E.; Romanovskii, N.N.; Kosmach, D.A.; Nikol'skii, D.N.; Nikiforov, S.L.; et al. The degradation of submarine permafrost and the destruction of hydrates on the shelf of east arctic seas as a potential cause of the 'Methane Catastrophe'. *Dokl. Earth Sci.* **2012**, *446*, 1132–1137. [CrossRef]